CHARACTERISING VOIDS AND WRINKLES IN CURVED CARBON FIBRE REINFORCED POLYMER PARTS USING μ-CT AND OPTICAL MICROSCOPY

Abhiram Ramesh[1], Mark Battley[2], Tom Allen[1] and Chris Hickey[3],

[1]Centre for Advanced Composite Materials, Department of Mechanical Engineering, University of Auckland, 314-390 Khyber Pass Road, Newmarket, Auckland, New Zealand
Email: aram067@aucklanduni.ac.nz, Web Page: http://www.cacm.auckland.ac.nz/en/cacm.html
[2]Centre for Advanced Composite Materials, Department of Engineering Science, University of Auckland, 314-390 Khyber Pass Road, Newmarket, Auckland, New Zealand
Email: m.battley@auckland.ac.nz, Web Page: https://unidirectory.auckland.ac.nz/profile/m-battley
[3]R&D and Design, Southern Spars Ltd, 15 Jomac Place, Avondale, Auckland, New Zealand
Email: chris.hickey@southernspars.com, Web Page: https://www.southernspars.com

Keywords: CFRP, defects, voids, wrinkles, micro-CT

Abstract
Defects such as voids and wrinkles may be formed in high performance carbon fibre reinforced polymer parts during manufacturing. These defects have been found to occur more frequently and in higher severities near areas of curvature, especially for thicker laminates, and have previously been shown to result in reduction of the elastic properties and strengths of parts. This study investigates techniques to identify and characterise these defects using micro-computer tomography, microscopy and image processing tools in order to improve their classifications and provide geometric information for analysis of their effects. Two independent techniques were developed during this study to characterise defects. The first method utilises micro-CT scans and is able to successfully determine features such as the shape, size & location of voids. The second method involves analysing micrographs taken using an optical microscope to automatically identify the edges of the plies within a laminate in order to characterise their wrinkle geometry. In addition to characterisation of the defects, these techniques will underpin further numerical and analytical studies into understanding the effects of voids and wrinkles on the performance of carbon fibre parts.

1. Introduction

High performance Carbon Fibre Reinforced Polymer (CFRP) parts used to replace sheet metal are often quite thin and have curvatures with relatively large radii. However, some CFRP structures such as aircraft wing boxes, wind turbine blades and yacht masts are highly loaded with very complex geometries. These parts are often thick and may potentially have corners with radii smaller the part's thickness. Thick laminates with smaller radii can often lead to internal defects during manufacturing and have shown to result in greater variability in the quality of the final part, as these areas are susceptible to an increased amount of porosity, discrete voids and fibre misalignments. The mechanical properties, particularly strength, may be reduced significantly depending on the size, location, geometry and type of defect induced [1-4]. During the manufacturing of carbon fibre composites, the formation of defects such as wrinkling of the fibres or voids within the matrix material have known to occur [5]. Manufacturing processes can be controlled to limit these defects, however this often leads to increased manufacturing costs and some defects can never be completely eliminated; especially voids.

It has been shown that thin laminates have higher tendency to bleed out excess resin than thick laminates during the curing phase of manufacturing. This means that excess resin which may cause voids by trapping any air or moisture within the laminate is removed during cure easily in a thinner laminate. Thicker laminates tend to trap air which cannot easily escape during de-bulking or curing. It is also more difficult to remove air, moisture and volatiles from the centre of thick laminates vertically (through-thickness), which may not be able to escape from the edges horizontally [6].

The two main types of defects found in prepreg based CFRP laminates are fibre misalignment and voids. Fibre misalignment may be defined as the deviation between the nominal and actual fibre direction. These may be in-plane, out-of-plane or a combination of the two. CFRP prepreg may contain misaligned fibres caused by the method of transportation and storage of the material between the supplier and part manufacturer [5, 7]. They may also be induced into a part during the layup or curing processes. Fibre misalignment can have a significant effect on the compressive stiffness and strength of unidirectional composites. The inter-laminar shear stresses which may arise due to fibre waviness has also been attributed to causing delamination and consequent failure of composites under loading [8]. Fibre wrinkles have shown a reduction in tensile strength of up to 40% in fibre reinforced polymers in some extreme cases. The fracture initiating in wrinkled regions are also able to propagate to seemingly defect free regions, making wrinkles a significant threat to components [9]. Voids are formed during the curing the stage of composites and may be caused by a number of different factors. These include; duration of cure, temperature, pressure, efficiency of vacuum bleeding of resin or inclusions of foreign substances such as moisture, air and dust. [10]. Mechanical properties such as compressive, shear, bending, transverse strengths and impact toughness properties are significantly affected by voids [11].

It has been well established in previous studies that defects cause a reduction in the performance of CFRP. However, there is not enough evidence to fully understand the effect that the characteristics of these defects, such as the aspect ratio (AR) & shape of voids, or the severity of fibre misalignment, have on the load carrying capabilities of CFRP parts. In order to conduct a thorough study into how parts are affected by various defects, it is necessary to accurately characterise their geometric features. Developing methods to identify and characterise typical voids and wrinkles will enable these properties to be used to create useful multiscale numerical models which may then be used to predict the behaviour of CFRP parts with various geometries of fibre wrinkling and/or voids.

2. Methodology

2.1. Materials and Manufacturing

Unidirectional prepreg CFRP with Toray - T700 standard modulus carbon fibres and Hankuk – RS4545S resin system was used to manufacture the specimens. All 0° plies used are 300 gsm and the rest of the plies are 150 gsm in order to achieve the highly directional laminate. The material was laid up with the stacking sequence: $[0/90/0/45/-45/0/-45/45/0/90/0/45/-45/0/-45/45/0/90/0/0/\pm45]_S$. This provided a ratio of 60 %, 30 % & 10 % of 0°, ±45° and 90° plies respectively. For structures carrying highly directional loads and need high strength and stiffness in the load direction such as a mast, this is a reasonable and representative ratio. Figure 1 (left) shows the local fibre orientations on a typical part from which the specimens are extracted. A female "U-shape" mould was constructed using aluminium with corner radii of 20 mm and sidewall angles of 100°. The cross sectional schematic of the mould used to manufacture specimens for this study is shown in Figure 1 (right). The prepreg material has a fibre volume fraction of 60% according the material supplier. During the lay-up process, the material was debulked after every third layer which is standard practice for these laminates. The panels were cured in an autoclave using a predefined temperature profile at 33.6 kPa pressure in order to allow for any excess resin to bleed and provide a final part with a high fibre volume fraction. The laminates were then cut into slices of various thicknesses depending on the type of imaging required. A diamond grit coated circular table saw with a blade thickness of 4 mm was used to slice the specimens into sections before a Beuhler IsoMet1000 precision saw was used to cut off the sidewalls and provide the final specimen as shown in Figure 2.

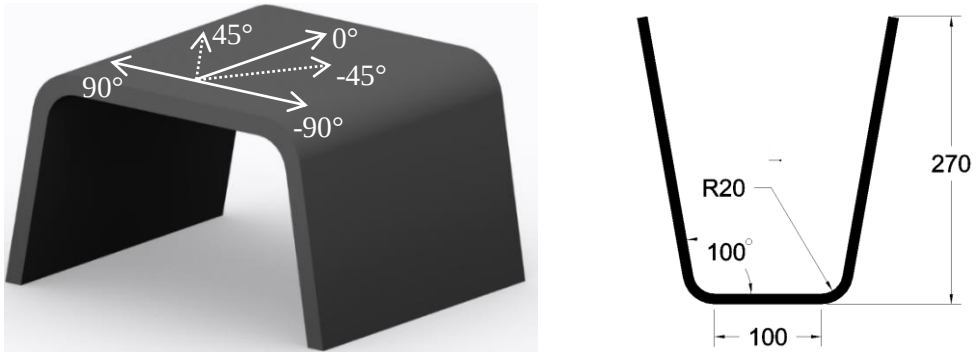

Figure 1. Fibre orientation on laminates (left), Cross section of aluminium mould with 20 mm corner radius (right)

In order to obtain micrographs of acceptable quality, the specimens are first prepared by cutting out the region of interest, potting them in West System 105 resin and then grinding & polishing them using Buehler – Ecomet 250 machine.

2.2. Imaging

Computer tomography (CT) uses penetrating radiation from multiple angles to produce images of specimen cross sections. CT results can include material properties such as density and discontinuities within the specimen [12]. A high resolution CT scan can provide details at a micrometre level and is referred to as micro-CT. Micro-CT scans were conducted on the corners of four specimens using Bruker SkyScan 1172 and 1272 scanners. The specimens were cut from the corners of the laminates (Figure 1) and typical specimen is shown in Figure 2. The results obtained from the scans provided enough detail to identify and analyse voids. However, the contrast between plies was not sufficient enough in the micro-CT results for them to be used to easily determine wrinkles present in the specimens. This meant that it was necessary to obtain two dimensional micrographs using a low magnification microscope to characterise wrinkles. A Leica – MZ16 stereomicroscope is used to produce micrographs of the polished specimens which are used to analyse the wrinkle characteristics of the corner regions of the CFRP panels.

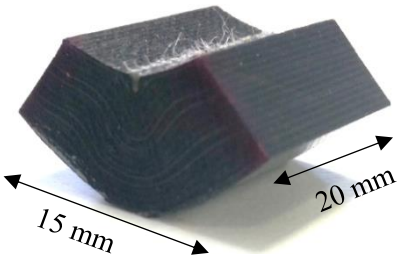

Figure 2. µ-CT Scan Specimen 01

2.3. Voids Characterisation

Curved CFRP parts were scanned and analysed to determine the shape, size, location and orientation of voids present within the laminate. Micro-CT x-ray scan results were exported as a series of TIFF images, where each image represents a single 2D x-ray projection. These results are reconstructed to form a 3D greyscale image stack in bitmap file format using NRecon (version 1.6.9.8). The analyses is then conducted using Matlab 2017 along with Matlab's Image Processing Toolbox.

Each image is initially rotated to match the required coordinate system by aligning an edge of the part to the edge of the image (Figure 3-2). Any excess pixels on the outside edges of the image are then cropped out (Figure 3-3). The image is then converted to a binary file based on an appropriate thresholding of the greyscale intensity. The threshold values have to be adjusted for different specimens because the pixel intensity may vary for each scan. It is also helpful to analyse the pixel intensity histogram so that it can be adjusted to provide better contrast between voids and the part itself. Once a suitable threshold value is established for each scan, then the greyscale images are converted to binary images and inverted so that any pixel with a value of 1 represents a void and all other pixels have a value of 0 (Figure 3-4). The noise is then eliminated in two steps; where the first step is to remove any small speckles which are below a certain number of pixels, and the second step is to close the image morphologically to reveal voids (Figure 3-5). Both these steps also require thresholding and verification to ensure that any speckles removed are not voids. Finally, after the voids are morphologically closed, the characteristics for the voids are determined for each image slice. The area, centroid location, length and width are measured for each of the voids in every image in the 3D stack, and the AR is then calculated. These steps are then repeated for each image slice to obtain void characteristic data for the entire part.

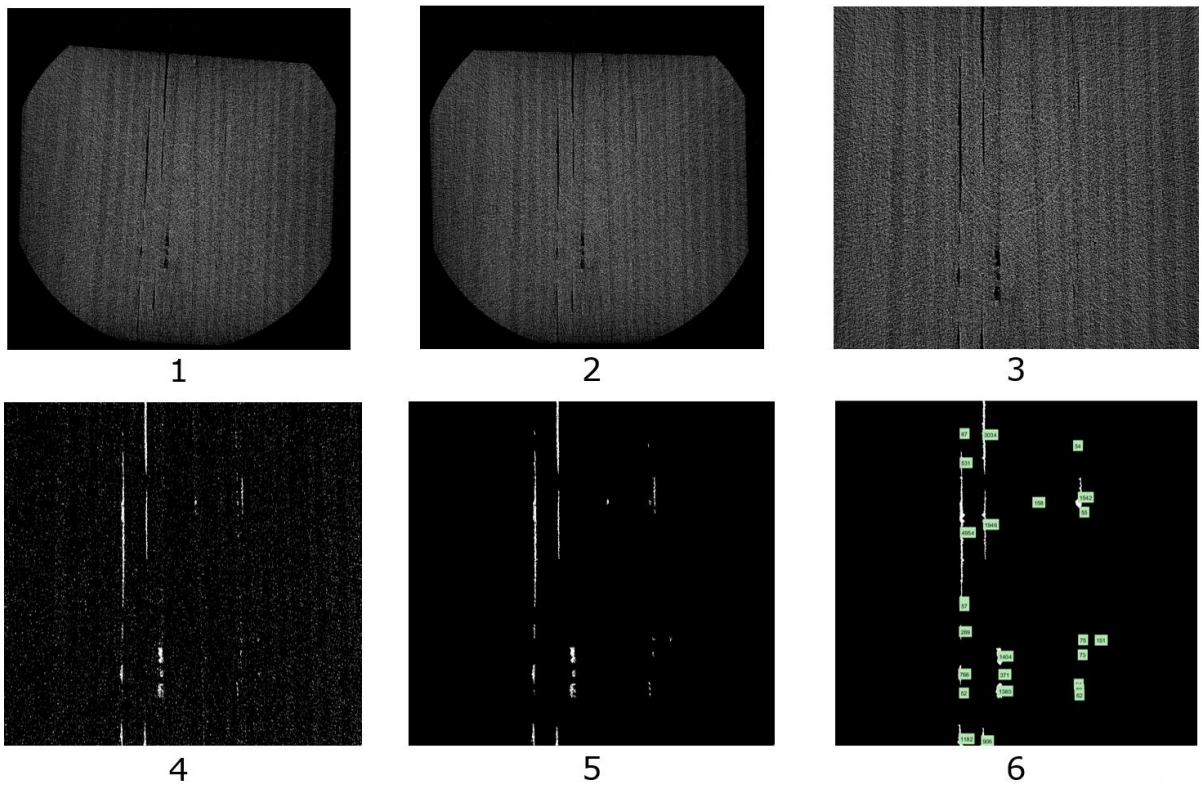

Figure 3. Original reconstructed image slice (1), rotated to correct orientation (2), cropped to region of interest (3), converted to binary and inverted (4), noise removed (5), and voids determined and analysed (6).

2.4. Wrinkles Characterisation

Images obtained from optical microscopy scans of wrinkled CFRP parts have been used to quantify the severity of wrinkles in the form of a sinusoidal or polynomial function. Since micrographs were used to determine wrinkling, it was only conducted for two dimensional slices at set intervals. The images captured using the microscope are 24-bit red-green-blue (RGB) colour images (Figure 4-1). After several attempts at identifying image processing techniques which could enhance the interply edges, it was determined that for the lighting and microscope used to obtain the micrographs the best results were

achieved by first isolating the red channel of the RGB image (Figure 4-2). Once the required channel was isolated, the image histogram was determined and stretched appropriately to improve contrast. The image is then converted to greyscale (Figure 4-3) and then to binary by applying a threshold for pixel intensity at each step. The lighting used for obtaining the micrographs can significantly affect the thresholding values and this needs to be accounted for during the analysis of each image. The binary image is then inverted to produce a pixel value of 1 at any features and 0 for the rest of the specimen (Figure 4-4).

The next step involves determining the edges of the plies. Typical methods of detecting edges rely on determining derivatives (first or second order) along the intensity profile of the image. Various edge detection techniques were investigated during the process of this study, such as Sobel, Canny, LoG and Prewitt [13]. The Sobel method was identified to be the most suitable method to use as it proved to produce the best results out of all the techniques that were attempted. Figure 4 shows progression of isolating ply edges and determining wrinkle characteristics from the microscopic image. The technique developed produces a series of two dimensional array where each set represents the coordinates for the pixels forming a ply edge. The data in each array is currently described using polynomials to express the absolute locations of each pixel representing the edges of plies. In order to be able to compare between specimens, these values need to be normalised so that each specimen is represented with a value which best describes the average deviation of its plies from its intended plane. This will be implemented in the next phase of the study.

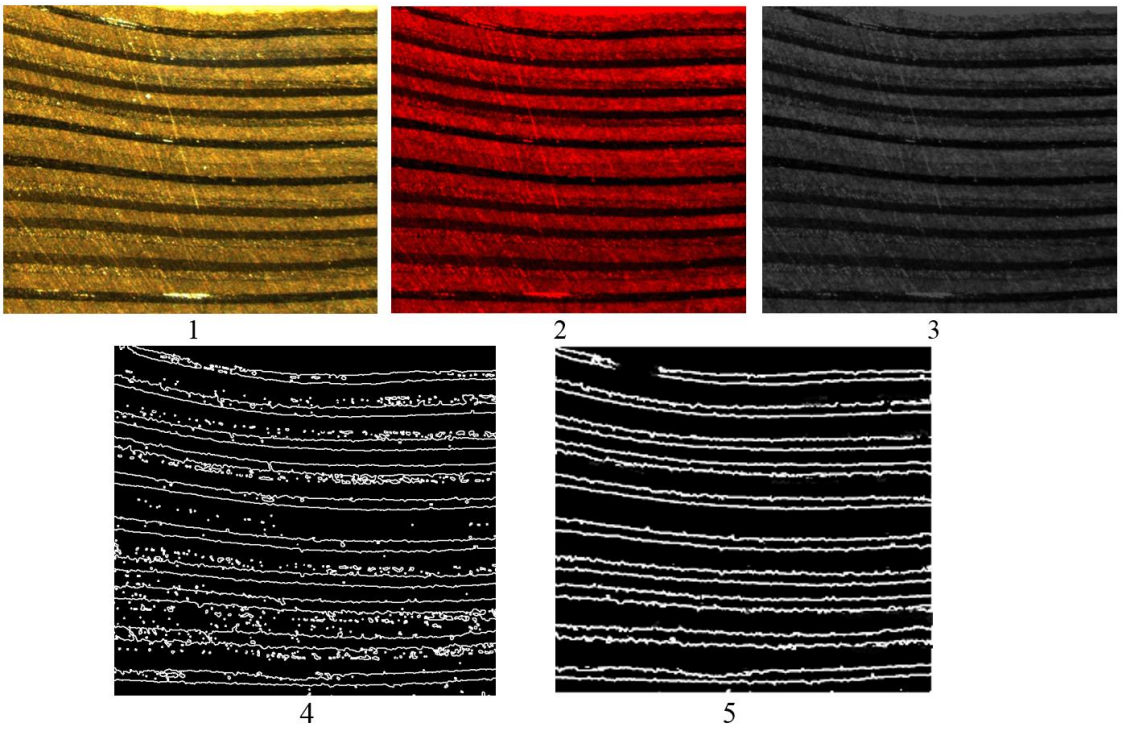

Figure 4. Original micrograph (1), red channel extracted (2), converted to greyscale (3), converted to binary (4) and noise removed (5).

3. Results and Discussion

Four specimens were scanned and analysed using the algorithm described in §2.3. Specimen 01 was manufactured first and scanned at a pixel resolution of 10 micrometres to develop the algorithm. Specimen 02, 03 and 04 were extracted from the same panel and scanned at a higher pixel resolution of 5.48 micrometres. The results for the four specimens are shown in Table 1.

Table 1. Summary of µ-CT Results for Void Analysis

Specimen 01	**x-y plane**	**x-z plane**	**y-z plane**
Void volume %	0.55%	0.55%	0.55%
Average void aspect ratio	21.56	34.25	8.01
Largest void length (mm)	8.34	24.09	9.92
Largest void width (mm)	1.01	0.18	0.26
Largest void area (mm^2)	5.98	1.76	1.93
Largest void location - x, y, z (mm from reference point)	15.21, 5.95, 3.82	9.87, 4.80, 4.32	19.39, 3.63, 4.41
Longest void (mm)	15.93	24.09	9.92
Widest void (mm)	1.14	0.30	0.45
Specimen 02			
Void volume %	4.70%	4.70%	4.70%
Average void aspect ratio	26.65	25.55	6.00
Largest void length (mm)	17.39	15.95	1.17
Largest void width (mm)	1.37	1.17	0.71
Largest void area (mm^2)	17.21	13.98	2.03
Largest void location - x, y, z (mm from reference point)	7.65, 6.39, 8.27	7.31, 1.61, 0.56	8.84, 6.10, 6.95
Longest void (mm)	17.97	17.56	3.94
Widest void (mm)	1.37	1.24	0.96
Specimen 03			
Void volume %	0.53%	0.53%	0.53%
Average void aspect ratio	21.45	30.80	7.68
Largest void length (mm)	9.87	13.94	1.61
Largest void width (mm)	1.00	0.33	0.35
Largest void area (mm^2)	6.44	2.75	0.34
Largest void location - x, y, z (mm from reference point)	10.67, 5.15, 2.65	9.18, 1.99, 0.19	8.16, 0.50, 1.79
Longest void (mm)	14.43	14.22	2.57
Widest void (mm)	1.14	0.34	0.35
Specimen 04			
Void volume %	0.00%	0.00%	0.00%
Average void aspect ratio	n/a	n/a	n/a
Largest void length (mm)	0.52	0.24	0.42
Largest void width (mm)	0.17	0.04	0.04
Largest void area (mm^2)	0.02	0.01	0.01
Largest void location - x, y, z (mm from reference point)	7.94, 7.74, 4.77	11.43, 3.88, 13.05	15.35, 7.69, 4.77
Longest void (mm)	0.52	0.25	0.48
Widest void (mm)	0.17	0.08	0.08

Small spherical porosities have lower aspect ratios than the larger voids and skew the results when analysing the average AR values of voids due to the larger number of smaller insignificant voids. So for the purpose of obtaining results that are qualitatively significant, the average AR values in Table 1 only consider voids larger than 0.1 mm^2. For Specimen 01, these are voids which are larger than 1000 pixels in total area and for the remaining specimens scanned at the higher resolution of 5.48 µm, voids larger than 3330 pixels in total area are analysed for determining their average AR.

As shown in Table 1, the specimens scanned showed void content ranging from 0.00% to 4.70%. The advantage of using micro-CT scans compared to methods such as acid digestion or matrix burn off tests is that the location of these voids, along with their sizes are accurately captured. The void shapes ranged from smaller needle shaped voids to large lens and cigar shaped voids. Most voids were at least 3 to 5 plies away from any outer surface. Since there was no material removed or missing during the manufacturing process, voids resulted in redistribution of the fibres around them which typically resulted in the thickening of the corner region. Aspect ratios were noticeably higher when looking at the 'xy' or 'xz' planes than the 'yz' plane, as shown in Figure 5. This indicates that the larger voids tend to be oriented in the x-direction.

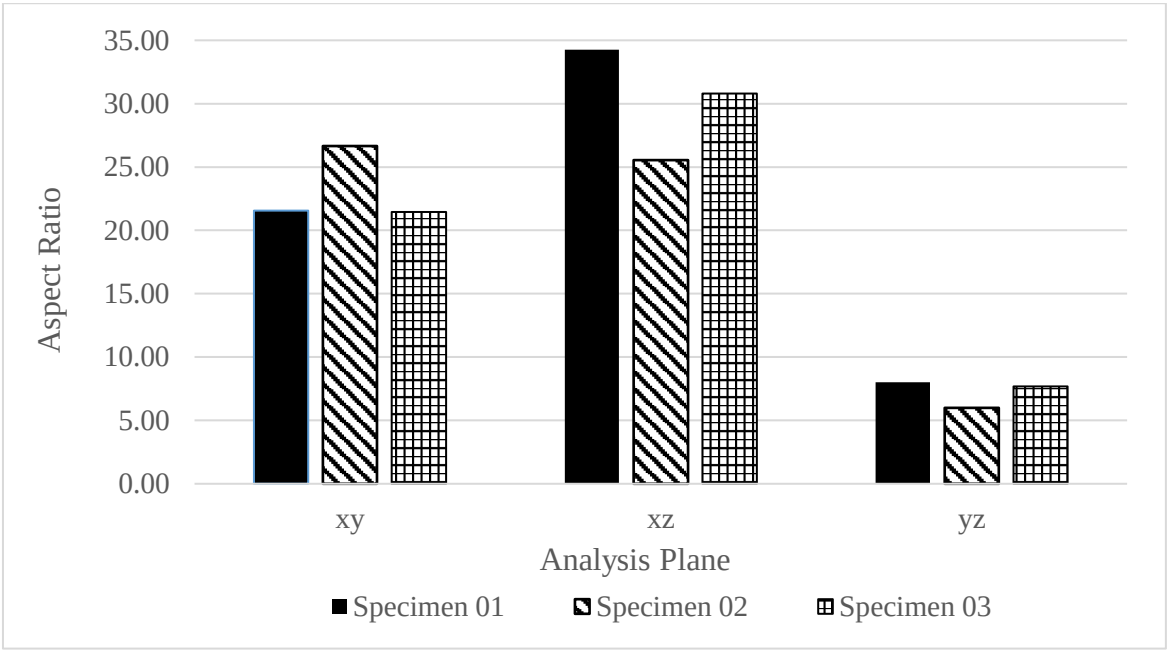

Figure 5. Average aspect ratio of voids larger than 0.1 mm^2 for all three planes of analyses

The current method analyses each individual 2D slice separately, limiting the amount of information that can be gathered from the scan. An improvement to this technique would involve stacking the images together and analysing the 3D matrix to provide volumetric data, which would be more representative of the voids of interest. However, the limitation to applying this technique is the amount of memory required to store the entire image stack dataset in order to analyse it. Pre-allocating values to a 3D matrix could potentially reduce the computational costs when compared to the current method which uses a 'FOR' loop to conduct the analysis.

4. Conclusion

Two independent processes were developed to characterise defects. The first method can successfully characterise defect features such as the shape, size & location of voids from micro-CT scan results, and the level of misalignment of plies. Large voids are typically cigar or lens shaped, lie along the x-direction and appear to be caused by ply bridging. The mechanisms that cause defects to occur during manufacturing results in larger wrinkles and voids to be fairly interactive. Large wrinkles were typically found to contain needle shaped voids adjacent to them.

The consistency of lighting for microscopy is important to obtain images that can be analysed using the algorithm developed during this study. The resolution of reconstructed micro-CT results need to be interpreted with care when using the technique discussed to ensure that results from scans of different pixel resolutions are comparable to each other.

More specimens need to be scanned using micro-CT and analysed to understand the characteristics of voids in corners. Scans of larger areas would be useful to gain better insight, but there are restrictions to this such as the amount of data created, the time required to conduct the scans and the costs associated with it. A large number of cross sections of corners will need to be imaged and analysed before establishing the fibre misalignment characteristics in curved regions. Once the details of these characteristics are defined, this data will then be used to create multiscale numerical models to determine the effect of the defect characteristics on the compressive behaviour of CFRP.

Acknowledgments

This study was funded by a grant provided by the Ministry of Business Innovation and Employment of New Zealand. Southern Spars Ltd supplied raw materials, manufacturing advice and logistical aid for this research.

References

[1] Shigang, A., et al., *Effect of manufacturing defects on mechanical properties and failure features of 3D orthogonal woven C/C composites.* Composites Part B: Engineering, 2015. **71**(0): p. 113-121.
[2] Nelson, J.W., D.S. Cairns, and T.W. Riddle. *Manufacturing Defects Common to Composite Wind Turbine Blades: Effects of Defects*. in *Proceedings AIAA Aerospace Science Meeting, Wind Energy Symposium, Orlando, FL*. 2011.
[3] Richards, J.M., et al., *Effects of manufacturing defects on the mechanical properties of carbon fibre reinforced polyethersulphone laminates.* Journal of Materials Science, 1989. **24**(2): p. 584-589.
[4] Wilkins, D.J. *Effects of defects in composite materials*. 1984. American Society for Testing and Materials.
[5] Potter, K., et al., *Variability, fibre waviness and misalignment in the determination of the properties of composite materials and structures.* Composites Part A: Applied Science and Manufacturing, 2008. **39**(9): p. 1343-1354.
[6] Campbell, F.C., *Chapter 6 - Curing: It's a matter of time (t) temperature (T) and pressure (P),* in *Manufacturing Processes for Advanced Composites*, F.C. Campbell, Editor. 2003, Elsevier Science: Amsterdam. p. 175-221.
[7] Potter, K., *2 - Manufacturing defects as a cause of failure in polymer matrix composites*, in *Failure Mechanisms in Polymer Matrix Composites*, P. Robinson, E. Greenhalgh, and S. Pinho, Editors. 2012, Woodhead Publishing. p. 26-52.
[8] Talreja, R., *5 - Manufacturing defects in composites and their effects on performance,* in *Polymer Composites in the Aerospace Industry*, P.E. Irving and C. Soutis, Editors. 2015, Woodhead Publishing. p. 99-113.
[9] Bloom, L.D., J. Wang, and K.D. Potter, *Damage progression and defect sensitivity: An experimental study of representative wrinkles in tension.* Composites Part B: Engineering, 2013. **45**(1): p. 449-458.
[10] Smith, R., *Composite Defects and Their Detection.* Materials Science and Engineering, 2009. **3**: p. 103-143.
[11] Olivier, P., J.P. Cottu, and B. Ferret, *Effects of cure cycle pressure and voids on some mechanical properties of carbon/epoxy laminates.* Composites, 1995. **26**(7): p. 509-515.
[12] Bossi, R.H.G., Gary E. ; Rempt, Raymond D., *X-Ray Computed Tomography for Emerging Aerospace Materials and Processes Development*. 1993, BOEING DEFENSE AND SPACE GROUP SEATTLE WA.
[13] Cufí, X., et al., *A review of image segmentation techniques integrating region and boundary information,* in *Advances in Imaging and Electron Physics*, P.W. Hawkes, Editor. 2003, Elsevier. p. 1-39.